

Using optical tweezer electrophoresis to investigate clay nanoplatelet adsorption on Latex microspheres in aqueous media

Vaibhav Raj Singh Parmar¹, Sayantan Chanda¹, Sri Vishnu Bharat Sivasubramaniam¹, and
Ranjini Bandyopadhyay^{1,*}

¹*Soft Condensed Matter Group, Raman Research Institute, C. V. Raman Avenue,
Sadashivanagar, Bangalore 560 080, INDIA*

November 11, 2024

Abstract

The adsorption of charged clay nanoplatelets plays an important role in stabilizing emulsions by forming a barrier around the emulsion droplets and preventing coalescence. In this work, the adsorption of charged clay nanoplatelets on a preformed Latex microsphere in an aqueous medium is investigated at high temporal resolution using optical tweezer-based single-colloid electrophoresis. Above a critical clay concentration, charged clay nanoplatelets in an aqueous medium self-assemble gradually to form gel-like networks that become denser with increasing medium salinity. In a previous publication [R. Biswas *et. al.*, **Soft Matter**, 2023, **19**, 24007-2416], some of us had demonstrated that a Latex microsphere, optically trapped in a clay gel medium, is expected to attach to the network strands of the gel. In the present contribution, we show that for different ionic conditions of the suspending medium, the adsorption of clay nanoplatelets increases the effective surface charge on an optically trapped Latex microsphere while also enhancing the drag experienced by the latter. Besides the ubiquitous contribution of non-electrostatic dispersion forces in driving the adsorption process, we demonstrate the presence of an electrostatically-driven adsorption mechanism when the microsphere was trapped in a clay gel. These observations are qualitatively verified via cryogenic field emission scanning electron microscopy and are useful in achieving colloidal stabili-

*Corresponding Author: Ranjini Bandyopadhyay; Email: ranjini@rri.res.in

sation, for example, during the preparation of clay-armoured Latex particles in Pickering emulsion polymerisation.

Keywords: Optical tweezer, Laponite clay suspension, Colloidal adsorption, Single-colloid electrophoresis.

1 Introduction

The attachment or adsorption of colloidal particles on solid surfaces in aqueous media decreases the overall interfacial energy of the system and is usually governed by screened electrostatic forces and non-electrostatic intermolecular forces [1–5]. Adsorption is a ubiquitous surface phenomenon with implications in surface coating, stabilisation, pollutant removal and heterogeneous catalysis [6, 7]. Colloidal clay nanoplatelets are characterised by shape-anisotropy and a high surface-to-volume ratio. Clays are useful in many processes, such as in additive manufacturing, and are used as rheological modifiers in industrial products. Previous studies on surfactant-free emulsion polymerization of Laponite clay-armored Latex microspheres demonstrated that Laponite clay nanoplatelets adsorbed on the surfaces of the microspheres to form monolayers that transformed into multilayers with increasing clay concentration [5, 8–10]. It was concluded from these experiments that non-electrostatic attractions between the clay and Latex particles resulted in clay adsorption.

Laponite, a synthetic hectorite clay belonging to the family of smectites, has a crystalline structure that is typical of 2:1 phyllosilicates [11, 12]. Each particle is disk-shaped with a diameter of 25–30 nm and a thickness of 0.92 nm [11]. Clay nanoplatelets are arranged in one-dimensional stacks or tactoids in dry powder form and have negatively charged faces. Neighbouring nanoplatelets in a tactoid share Na^+ ions in the intergallery spaces. In an aqueous medium, the Na^+ ions diffuse out to the bulk water medium due to the build-up of an osmotic pressure difference between the intergallery spaces and the bulk. This induces an electrostatic repulsive force between the negatively charged faces of the clay nanoplatelets, which results in tactoid swelling and, eventually, nanoplatelet exfoliation [11]. If the medium $\text{pH} < 11$, the clay nanoplatelets have weak positively charged rims due to the protonation of magnesia groups and experience rim-to-face electrostatic attraction, and face-to-face and rim-to-rim electrostatic repulsion [13, 14]. They also interact via non-electrostatic dispersion forces such as van der Waals attraction between their faces and rims [13, 14].

Aqueous Laponite clay suspensions phase-separate at concentrations below 1% w/v [15] and self-

assemble into attractive gels with system spanning microstructures at clay concentrations between 1% w/v to 4.0% w/v [16]. Due to tactoid swelling, nanoplatelet exfoliation and the gradual self-assembly of the heterogeneously charged Laponite nanoplatelets in overlapping coins and house of cards configurations to form system-spanning gel networks, clay suspensions above 1% w/v undergo physical aging. This leads to a continuous increase in the elastic and viscous moduli of the suspension with time as physical aging progresses [13,16–19]. Increase in salinity of the aqueous medium accelerates the formation of percolated gel-like networks in the suspension medium [13,14,20]. Adding peptizing agents such as tetrasodium pyrophosphate (TSPP) inhibits network formation as rim-to-face electrostatic attractions reduce considerably due to adsorption of negatively charged pyrophosphate ions onto the positively charged rims of the Laponite platelets [21,22]. It has been reported that Laponite suspensions exhibit nematic order at concentrations above 4% w/v [23].

This paper proposes a new technique to study the adsorption of charged Laponite nanoplatelets on the surfaces of similarly charged Latex microspheres. Previous experiments had demonstrated that an optically trapped microsphere executes oscillatory motion due to electrophoresis in an applied alternating electric field [24, 25]. An externally imposed oscillatory electric field of known strength could therefore, in principle, be used to measure the electrical force (= effective charge \times electric field) acting on an optically trapped microsphere to extract the effective charge on the latter. This technique, known as optical tweezer-based single-colloid electrophoresis, has been used to determine the charges on colloidal particles and biological samples in polar and non-polar media [26–34] with a resolution of a single elementary charge [29,30], for measuring the concentration of a target protein in a buffer [32,33] and to investigate the adsorption of polymers on a colloidal silica sphere [34,35].

In a previous contribution, some of us had reported the adsorption of clay nanoplatelets on a trapped Latex microsphere in oscillatory active microrheology measurements [18]. We had also demonstrated that the mechanical response of the microscopically heterogeneous clay suspension depends on the microsphere diameter. In the present work, we visualised Latex microspheres suspended in Laponite clay suspensions using cryogenic field emission scanning electron microscopy (cry-FESEM) and identified the bright spots on the microsphere surfaces as adsorbed clay nanoplatelets. The standard deviation of the intensity distribution on the microsphere surface was calculated to quantify the extent of nanoplatelet adsorption. The addition of sodium chloride (NaCl) or TSPP in the suspension medium was seen to significantly influence the adsorption process. The kinetics of Laponite nanoplatelet adsorption on a trapped Latex microsphere in an aqueous medium were next estimated using optical

tweezer-based single-colloid electrophoresis experiments. Adsorption of clay nanoplatelets results in the transfer of net charges to the microsphere surface. We characterise the nanoplatelet adsorption process by measuring the temporal evolutions of the effective surface charges and the hydrodynamic drags on microspheres trapped in clay suspensions with different salt contents. We observed that the effective surface charge and hydrodynamic drag show similar increasing trends with increasing clay concentration, NaCl concentration and time. We identified two distinct mechanisms that drive the adsorption process. Besides rapid adsorption due to non-electrostatic dispersion forces, we also observed slower and more gradual adsorption, driven by the weakening of electrostatic repulsion between the microsphere and the faces of the self-assembled Laponite nanoplatelets at later times.

We successfully tuned the adsorption of Laponite clay on a Latex microsphere by incorporating controlled amounts of NaCl or TSPP in the suspension medium. The extent of nanoplatelet adsorption, as quantified from cryo-FESEM images, agrees with our effective surface charge measurements extracted from optical tweezer-based single-colloid electrophoresis experiments. The findings of our study are useful in stabilising colloidal clay-armoured Latex particles in various scenarios, such as during Pickering emulsion polymerization [5, 8] and in estimating the real-time adsorption efficiency of patchy particles [36].

2 Materials and methods

2.1 Sample preparation

Experiments were performed with aqueous suspensions of Laponite[®] XLG (BYK Additives Inc.), a synthetic clay powder constituted by disk-shaped clay nanoplatelets with a diameter of 25-30 nm and thickness of 0.92 nm. Since Laponite[®] is hygroscopic, the absorbed moisture was removed by baking the clay powder in an oven for 18-24 hours at 120°C. Slightly negatively charged polystyrene Latex microspheres were procured from Bangs Laboratories, Inc. NaCl (LABORT Fine Chem Pvt. Ltd) or TSPP (E. Merck (India) Ltd) were mixed in ultrapure Milli-Q water (Millipore Corp., resistivity = 18.2 MΩ-cm) to prepare aqueous solutions of pre-determined concentrations. A fixed quantity of dried Laponite[®] powder was added to 50 ml MilliQ water or to NaCl or TSPP solutions prepared as above. The mixtures were stirred continuously for 40 minutes to prepare homogeneous suspensions. 10 ml of a freshly prepared suspension was filtered using a syringe filter of pore size 0.45 μm (SLHAR33SS Millex). A very dilute suspension of Latex microspheres of diameter 1.0 μm was added to the filtered

Laponite[®] suspension and stirred for another 5 minutes. The suspensions thus prepared were used for cryo-FESEM and optical tweezer electrophoresis measurements.

2.2 Cryogenic field emission scanning electron microscopy (cryo-FESEM)

Freshly prepared Laponite[®] suspensions with added Latex microspheres were loaded in capillary tubes (Capillary Tube Supplies Ltd, UK) of diameter 1 mm. The tubes were subsequently sealed at their two ends and left undisturbed for 90 minutes at room temperature ($24\pm 2^\circ\text{C}$). The instant at which the tube was sealed was recorded as the start of the experiment (aging time $t_w = 0$). The samples in the tubes were next vitrified in liquid nitrogen slush at -190°C (PP3000T Quorum technology) and transferred to a vacuum chamber. A precision knife was used to cut the sample, which was then sublimated for 15 min at -90°C . A gold coating of thickness ≈ 5 nm was applied to the sample surface to ensure good image contrast. Finally, the samples were transferred to the cryo-chamber, maintained at a temperature of -190°C , for imaging. Back-scattered secondary electrons were used to reconstruct the surface images of the samples. Raw grayscale cryo-FESEM images of trapped Latex microspheres are displayed in Fig. S1 of the supplementary information. Python, version 3.9.13, in Jupyter Notebook was used to characterise the extent of adsorption of clay nanoplatelets on the microsphere by calculating the standard deviation of the pixel intensity distribution of the cropped grayscale microsphere image. A statistical analysis of the intensity profile of an image of a microsphere embedded in a 2.5% w/v Laponite suspension at $t_w = 90$ mins (Fig. S2) reveals that a majority of the bright spots in the grayscale cryo-FESEM image, including the ones seen on the microsphere surface, correspond to individual Laponite clay nanoplatelets and small aggregates.

2.3 Sample cell for optical tweezer-based single-colloid electrophoresis

The sample cell, schematically illustrated in the inset of Fig. 1, was prepared using a glass slide, a #1.0 coverslip (thickness ≈ 150 μm , Blue Star, India), and two copper strips, each of thickness ≈ 80 μm . The copper strips act both as electrodes and spacers. The glass slides and coverslips were adhered to each other using a multi-purpose sealant (Dowsil 732). Since each sample cell had a slightly different electrode separation, d , we measured the distance between the electrodes in each cell using a digital vernier calliper ($\Delta d = 0.01$ mm) and reported 4.80 mm $< d < 5.30$ mm for the different sample cells used in this work.

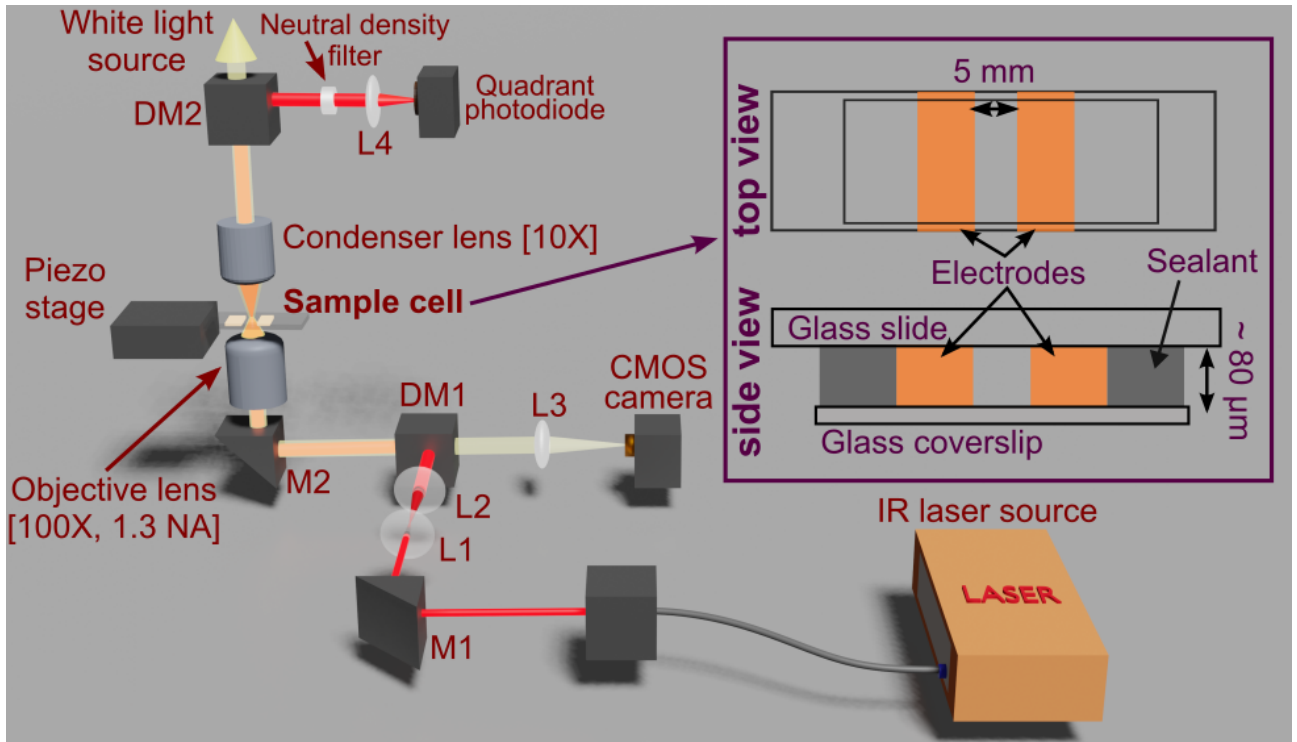


Fig. 1: Schematic illustration of the optical tweezer setup used for single-colloid electrophoresis experiments. M1 and M2 are mirrors, DM1 and DM2 are dichroic mirrors, L1, L2, L3 and L4 are achromatic doublet lenses of focal lengths 35 mm, 150 mm, 200 mm and 35 mm respectively. The infrared laser beam is indicated in red. (Inset) Schematic illustrations of the top and side views of the sample cell.

2.4 Optical tweezer setup

Figure 1 schematically illustrates the optical tweezer (OT, ThorLabs OTKB module) setup used to perform single-colloid electrophoresis experiments. A linearly polarized infrared laser (YLR-5-1064-LP, IPG Photonics) with a wavelength of 1064 nm and a Gaussian beam profile (TEM₀₀ mode) was used for trapping. After reflecting from the guiding mirror (M1), the beam was expanded using a combination of two lenses (L1 and L2) to overfill the back aperture of the objective lens. The expanded beam passed through the dichroic mirror (DM1) and was guided to the oil immersion objective (100X, 1.3 NA Olympus) to form a diffraction-limited spot. The gradient forces produced by the focused laser beam trapped the microsphere in three dimensions. The scattered beam was collected using a condenser lens (10X, Nikon). The reflected beam from the dichroic mirror (DM2) was attenuated by a neutral density filter and focussed using the lens (L4) on a quadrant photodiode (QPD - PDQ80A, Thorlabs). The quadrant photodiode (QPD) was kept at the back focal plane of the condenser and used to detect nanometer-scale deflections of the trapped Latex microsphere [37, 38]. The output from the QPD was recorded using Labview 2021 with a data acquisition device (DAQ, NI USB-

6218, National Instruments) at a sampling rate of 30 kHz. The protocols for QPD calibration and conversion of microsphere deflections to power spectral density (PSD) of the position fluctuations of the trapped microsphere were implemented using MATLAB 2024a as described in Figs. S3 and S4 of the supplementary information. The stiffnesses of the optical trap at various laser powers, determined by trapping Latex microspheres in water in the absence of an electric field, are displayed in Fig. S5 of the supplementary information. In this work, the laser power used was 330 mW and the measured trap stiffness was $50.61 \text{ pN}/\mu\text{m} \pm 0.37 \text{ pN}/\mu\text{m}$.

For each single-colloid electrophoresis experiment, a freshly prepared Laponite clay suspension with Latex microspheres was loaded in the sample cell which was then placed on a piezo-controlled stage. The electrodes of the sample cell were connected to a frequency generator (Agilent 33220A). A sinusoidal electric field was applied at $t_w = 0$ minutes and maintained throughout the experiment. As the viscoelasticity of the clay suspension increased rapidly with clay concentration and age, the position fluctuations of the trapped microsphere became increasingly more difficult to resolve, rendering the trap ineffective. We chose the concentration and age ranges of the Laponite suspension media accordingly, and retained only those experiments wherein the corner frequency, f_c , of the PSD of microsphere position fluctuations was greater than 100 Hz.

2.5 Measurement of the effective surface charge on the Latex microsphere

The motion of a microsphere in an optical trap in the presence of a uniform AC electric field, $E(t) = E_0 \sin(2\pi f_{AC}t)$ applied along the \hat{x} direction (Fig. 2(a)), is described by the Langevin equation for a periodically driven Brownian oscillator [26, 32, 39]:

$$m\ddot{x}(t) + \gamma [\dot{x}(t) - v_{eo}] + \kappa x(t) = F_T(t) + F_E(t) \quad (1)$$

Here, m is the mass of the trapped microsphere, $x(t)$ is the \hat{x} component of the centre of mass motion of the microsphere, γ is the Stokes drag coefficient, v_{eo} is the electro-osmotic flow velocity of the medium, κ is the trap stiffness, F_E is the electrical force and $F_T(t) = \sqrt{2\gamma k_B T} \xi(t)$ is the random thermal force. In the expression for $F_T(t)$, k_B is the Boltzmann constant, T is the absolute temperature and $\xi(t)$ is the zero-mean delta-correlated white noise with $\langle \xi(t) \rangle = 0$ and $\langle \xi(t)\xi(t') \rangle = \delta(t-t')$. As discussed earlier, we trapped the microsphere in clay suspensions of small ages to ensure trap effectiveness. Since these samples were predominantly liquid-like, the zero-mean delta-correlated white noise approximation

holds for our experiments. In addition, as the applied electric field was expected to rupture some of the fragile microstructures in the clay suspension, the optically trapped Latex microsphere was modelled as a Brownian particle.

For an applied AC electric field of strength E_0 and frequency f_{AC} , $F_E(t) = Q_{eff}E_0 \sin(2\pi f_{AC}t + \phi)$, where $Q_{eff} = eZ_{eff}$ is the effective charge on the surface of the trapped microsphere and ϕ is the phase difference between the centre of mass position of the microsphere and the applied field. In the expression for Q_{eff} , e is the elementary charge and Z_{eff} is the effective number of elementary charges on the trapped microsphere. A previous study has shown that at sufficiently high AC frequencies, the contribution of electro-osmosis to the motion of a trapped Latex microsphere can be neglected [40]. We have applied an AC electric field of frequency $f_{AC} = 7.992$ kHz while trapping the microsphere at least $7 \mu\text{m}$ away from the surface. Considering $v_{eo} \approx 0$ and an overdamped limit, $m\ddot{x}(t) = 0$ since Reynold's number $< 10^{-4}$ in all our experiments, a Fourier transform of Eqn. (1) yields the one sided power spectral density, $S_{xx}(f)$, which describes the oscillation amplitude of the trapped microsphere: [26, 32, 39]:

$$S_{xx}(f) = \frac{k_B T}{\pi^2 \gamma} \frac{1}{f^2 + f_c^2} + \frac{k_B T}{\kappa} \Gamma^2 \delta(f - f_{AC}) \quad (2)$$

The first term in Eqn. (2) is a Lorentzian function with a corner frequency $f_c = \kappa/2\pi\gamma$ and represents the Brownian dynamics of the trapped microsphere. The second term in Eqn. (2) represents the oscillatory motion of the microsphere in the alternating electric field and is characterised by a δ -peak at $f = f_{AC}$. The dimensionless parameter Γ^2 is proportional to the ratio of the mean-square electrical and Brownian forces: [26, 32, 39]

$$\Gamma^2 = \frac{1}{1 + (f_{AC}/f_c)^2} \frac{e^2 Z_{eff}^2 E_0^2}{2k_B T \kappa} \quad (3)$$

Equation (3) can be rearranged to yield the effective surface charge on the trapped microsphere [39]:

$$eZ_{eff} = \frac{\Gamma}{E_0} \sqrt{2k_B T \kappa \left[1 + \left(\frac{f_{AC}}{f_c} \right)^2 \right]} \quad (4)$$

We have computed the Fourier transform of the trajectory of the trapped microsphere, $x(t)$, obtained from our single-colloid electrophoresis experiment (representative data displayed in Fig. 2(b)),

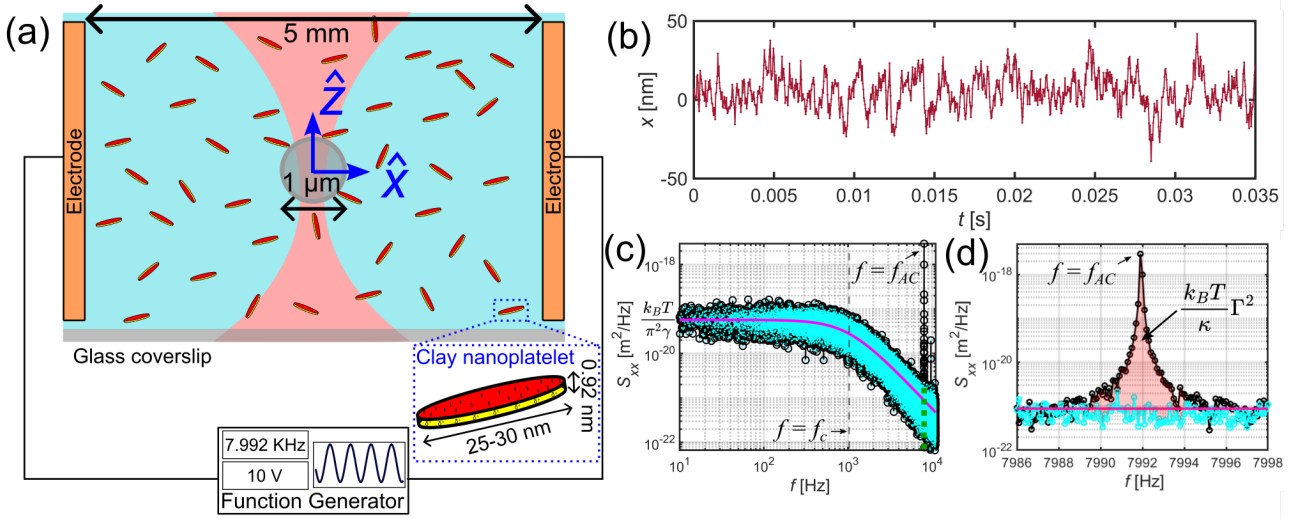


Fig. 2: Schematic illustration of a slightly negatively charged Latex microsphere of radius $1.0 \mu\text{m}$ optically trapped in a Laponite clay suspension. The AC electric field was applied along the \hat{x} direction. (b) A representative trajectory of a microsphere trapped in water in an AC electric field. (c) Power spectral density, $S_{xx}(f)$, and (d) a zoomed-in view of the peak centred at $f_{AC} = 7.992 \text{ kHz}$. The dimensionless parameter Γ^2 is computed from the area under the peak shown in pink.

to obtain the PSD, $S_{xx}(f)$ (Fig. 2(c)). Drag-dominated Brownian forces overcome optical forces at frequencies higher than f_c , therefore, $S_{xx}(f) \sim 1/f^2$ at $f > f_c$. Furthermore, an additional contribution to the PSD, arising from microsphere oscillation in the applied AC electric field, is clearly visible as a sharp peak at the applied AC frequency $f_{AC} = 7.992 \text{ kHz}$ (green dashed line in Fig. 2(c)). Fig. 2(d) shows a zoomed-in view of the peak centred around $f_{AC} = 7.992 \text{ kHz}$. Electric power is therefore distributed within a narrow frequency range under the peak, the finite height and width of which (pink shaded area in Fig. 2(d)) arises from the discrete data acquisition process. Following previous work, we computed the electric power by estimating the area under the peak [41] at $f = f_{AC}$ (pink shaded area in Fig. 2(d)) using Eqn.(2).

The corner frequency, f_c , was estimated by fitting a Lorentzian function to $S_{xx}(f)$ (Fig. 2(c)). The areas under the sharp peaks were calculated using the trapezoidal numerical integration procedure, after subtracting the thermal baseline (red line in Fig. 2(d)). Since trap stiffness κ and room temperature T are known, the electrical power transferred during the adsorption process was calculated using Eqn. (2). In all our electrophoresis experiments, the oscillatory motion of the trapped microsphere in the applied electric field was substantially smaller than its overdamped Brownian motion in the viscous medium, therefore $\Gamma^2 < 1$ (Fig. 3(a)). Finally, the Stokes drag coefficient, $\gamma = \kappa/2\pi f_c$, was also calculated.

Before acquiring data for single-colloid electrophoresis of a microsphere trapped in clay suspensions,

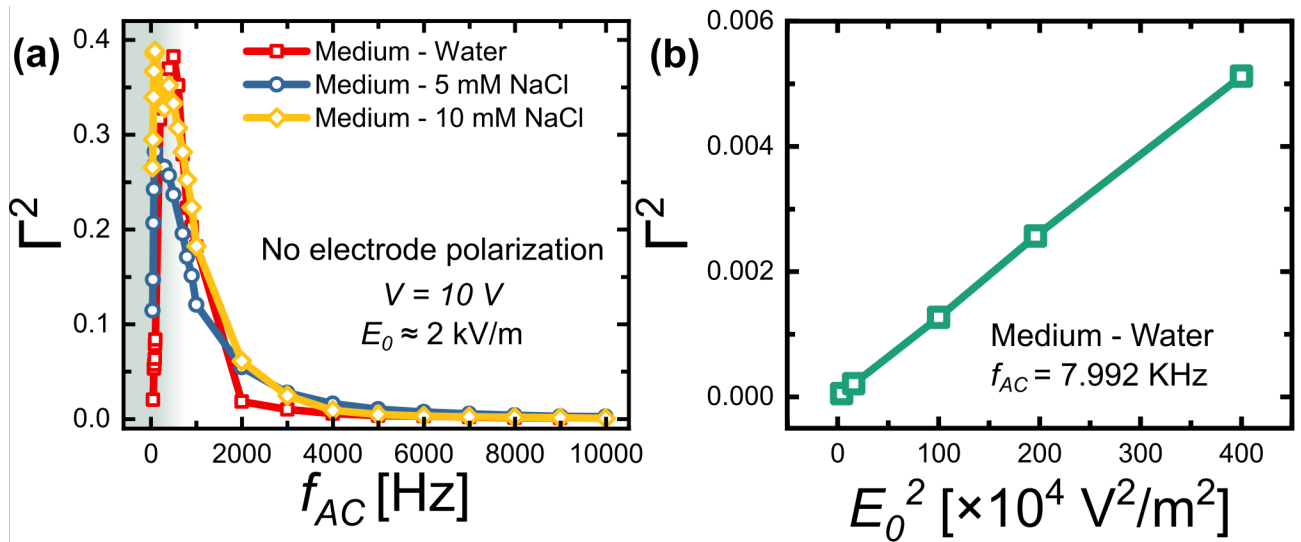


Fig. 3: (a) Dimensionless parameter Γ^2 , proportional to the ratio of mean-square electric and Brownian forces, as a function of AC field frequency, f_{AC} , for a microsphere trapped in aqueous media with different ionic contents. (b) Γ^2 as a function of the square of electric field strength, E_0^2 , for the microsphere trapped in water.

we validated our setup by trapping the microsphere in an aqueous medium. We measured the dimensionless parameter Γ^2 as a function of electric field strength, E_0 , and frequency, f_{AC} . The observed frequency-dependent variation of Γ^2 at a fixed AC electric field is plotted in Fig. 3(a) for different ionic contents in an aqueous medium. The initial increase in Γ^2 at low f_{AC} arises from a reduction in the electrode polarisation-induced screening of the applied electric field [41]. The trapped microsphere experienced enhanced viscous damping when f_{AC} was increased, with Γ^2 decreasing to values $\sim O(10^{-3})$ when $f_{AC} \sim O(\text{kHz})$. In Fig. 3(b), Γ^2 of a microsphere trapped in water is plotted *vs.* E_0^2 at $f_{AC} = 7.992 \text{ kHz}$. As predicted by Eqn. (3), a linear dependency of Γ^2 on E_0^2 is observed. For our subsequent electrophoresis experiments, we chose $E_0 \approx 2 \text{ kV/m}$.

3 Results and Discussion

3.1 Observation of clay nanoplatelet adsorption on a Latex microsphere using Cryo-FESEM

The physical aging behaviour of Laponite clay suspensions has been quantified extensively in several rheological studies by measuring the time-evolution of suspension viscoelasticity both in the presence and absence of externally added salts [14,20]. It was seen that while clay aging is fastest in the presence

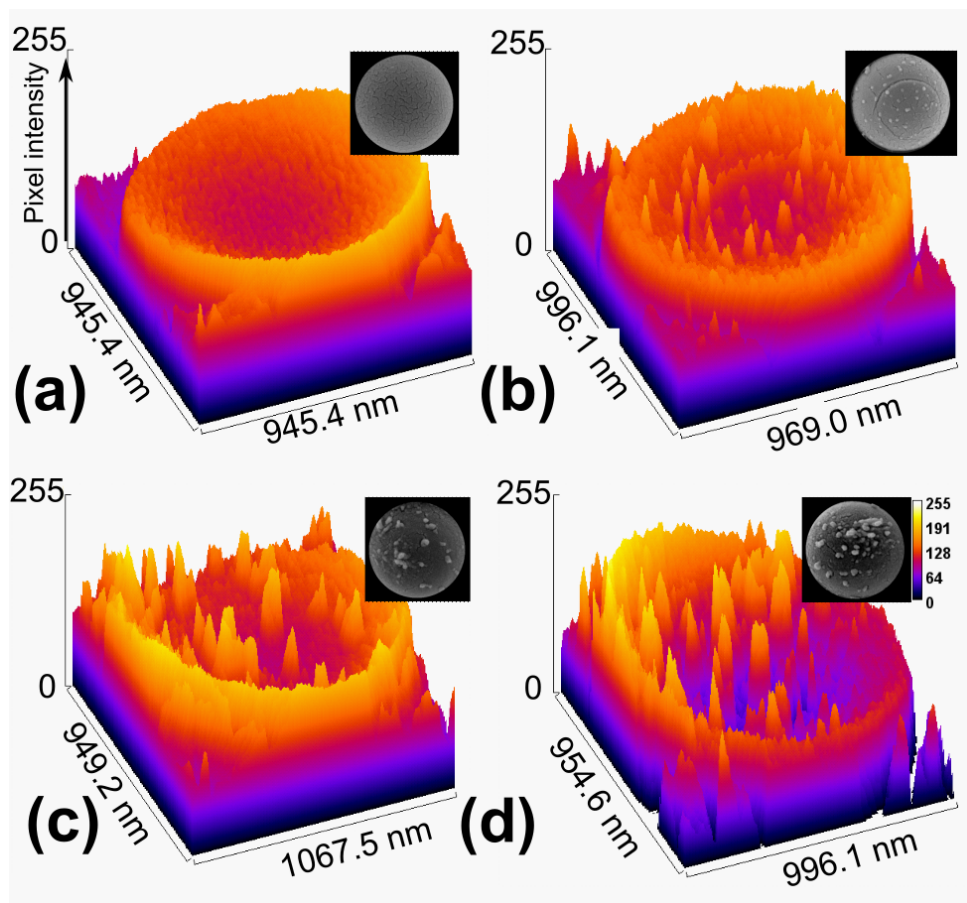


Fig. 4: Cropped cryo-FESEM images (insets) and the corresponding pixel intensity variation maps of the surfaces of Latex microspheres of diameter $1.0 \mu\text{m}$ in (a) water, (b) 2.5% w/v aqueous Laponite suspension, (c) 2.5% w/v aqueous Laponite suspension in the presence of 1.25 mM TSPP and (d) 2.5% w/v aqueous Laponite suspension in the presence of 1.25 mM NaCl at an aging time $t_w = 90$ minutes.

of NaCl, it could be completely suppressed by adding an adequate quantity of TSPP to the aqueous medium [22, 42].

To verify the adsorption of Laponite clay nanoplatelets on Latex microsphere surfaces in different ionic conditions, we first conducted direct visualisation via cryo-FESEM. All the cryo-FESEM experiments displayed here were performed at a fixed aging time, $t_w = 90$ minutes. Grayscale cryo-FESEM images of microspheres embedded in water or clay suspensions in various ionic conditions are displayed in Fig. S1. We cropped these images using a masking algorithm in Python to focus on the adsorption of clay nanoplatelets on the surfaces of the Latex microspheres. Pixel intensity variations obtained from the grayscale images of the microsphere surface, with the corresponding cropped images in the inset, are presented in Fig. 4. When the microsphere was suspended in water, a smooth surface texture was observed, as displayed in Fig. 4(a). When the microsphere was embedded in a clay suspension of

concentration 2.5% w/v, several bright spots were observed on its surface, as displayed in Fig. 4(b). The histogram of the size distribution of the bright spots is plotted in Fig. S2(b) of the supplementary information. The histogram shows peaks at ≈ 25 nm and 50 nm, which correspond respectively to the lateral dimensions of individual Laponite nanoplatelets and small particle clusters.

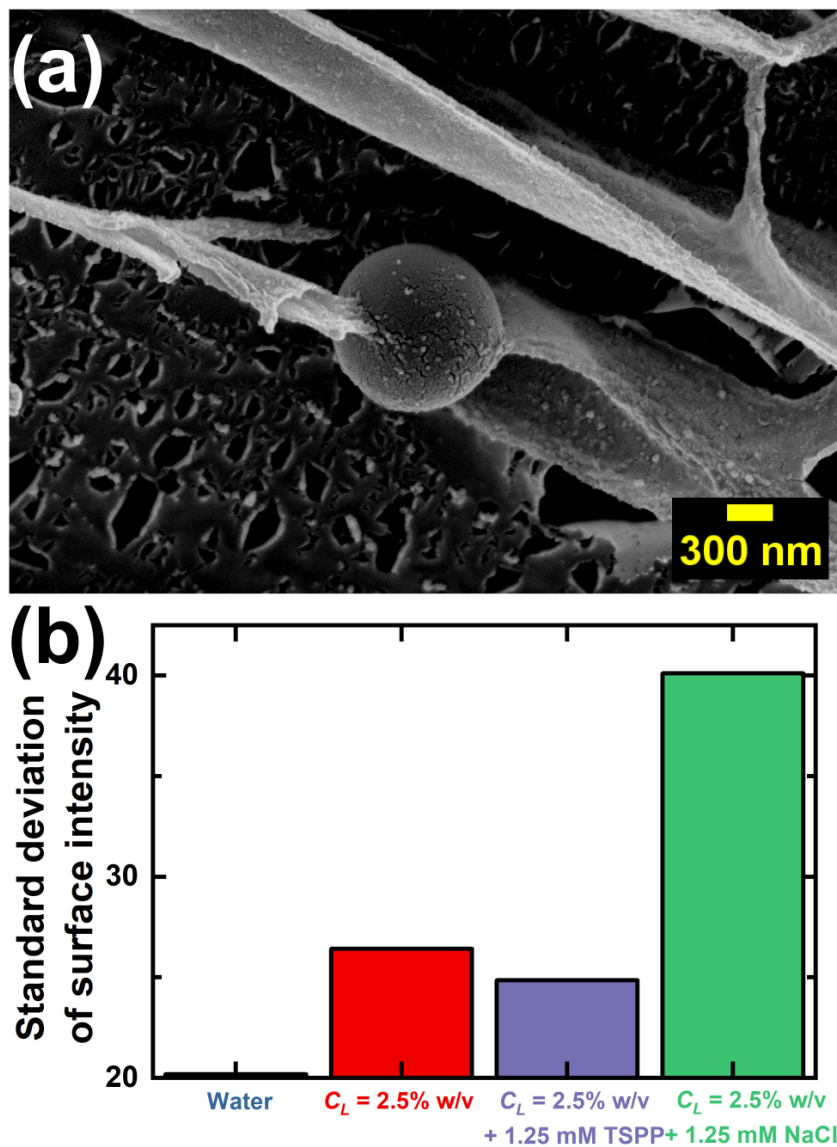


Fig. 5: (a) Cryo-FESEM image of a Latex microsphere attached to the strands of an evolving Laponite clay gel network. (b) Standard deviations of surface intensities in arbitrary units for Latex microspheres embedded in water or clay suspensions.

Fig. 4(c) shows the intensity variation map on the microsphere surface due to the adsorption of clay nanoplatelets in the presence of tetrasodium pyrophosphate (TSPP). It is known that the attachment of pyrophosphate ions ($P_2O_7^{4-}$) to the rims of Laponite clay nanoplatelets can reduce or neutralise the positive charges or even render negative charges on the rims [22]. Enhanced ad-

sorption of clay nanoplatelets is clearly evident from Fig. 4(c) for this system, which suggests that non-electrostatic dispersion forces initiate the adsorption process. In the presence of NaCl, an increase in the number of adsorbed nanoplatelets on the microsphere surface is evident from Fig. 4(d). A higher number density of Na^+ and Cl^- ions in the suspension medium screens the electrostatic repulsion between the nanoplatelets and microsphere. As a consequence, there is a relatively higher probability of a nanoplatelet approaching very close to (within $O(10 \text{ nm})$ of) the microsphere surface. Under these conditions, acceleration in the Laponite adsorption process is expected due to short-range non-electrostatic dispersion interactions. It was shown previously that increasing NaCl concentration in the medium leads to an increased rate of adsorption of nanoplatelets on a Latex microsphere and the eventual formation of nanoplatelet multilayers [5, 8]. As discussed earlier, Laponite clay suspensions form a gel at concentrations above 1% w/v [13]. Interestingly, we observed in an earlier study that the evolving gel networks can also attach to the trapped microsphere [18]. A representative image is shown in Fig. 5(a).

In summary, we determined that the dominant mechanism driving the adsorption process is non-electrostatic dispersion forces. Since the adsorbed nanoplatelets appear as bright spots, the standard deviation in intensity variation profiles on the surface of the microsphere, as displayed in Fig. 4, should give us valuable information on the extent of nanoplatelet adsorption. We therefore quantified the adsorption of Laponite nanoplatelets in different ionic conditions of the suspension medium by computing the standard deviations of the pixel intensities on the surfaces of the Latex microspheres. Representative bar plots are displayed in Fig. 5(b). A higher standard deviation of the pixel intensities in the presence of NaCl confirms a very high degree of nanoplatelet adsorption.

3.2 Quantifying the kinetics of nanoplatelet adsorption on a trapped Latex microsphere using single-colloid electrophoresis measurements

We next quantified the clay adsorption process by implementing optical tweezer electrophoresis. Since the adsorption of Laponite clay nanoplatelets transfers net charges to the surface of a Latex microsphere, we measured the surface charge of a single optically trapped microsphere as a function of clay suspension aging time, t_w , to gain insights into the kinetics of the adsorption process. Thermal fluctuations of optically trapped microspheres in Laponite clay suspensions were monitored to simultaneously measure the effective surface charge and Stokes drag on the former. Figure 6(a) shows the power spectral densities, $S_{xx}(f)$, calculated from the experimental trajectories of a microsphere trapped in

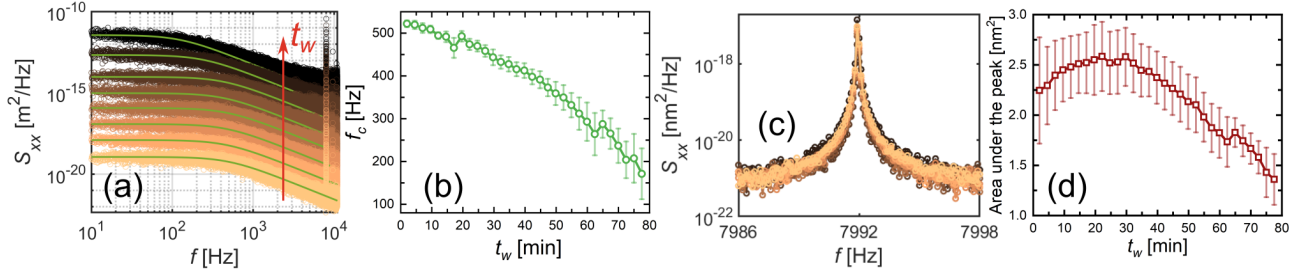


Fig. 6: (a) Power spectral densities (PSDs), $S_{xx}(f)$, of a Latex microsphere optically trapped in a Laponite clay suspension of concentration 2.5% w/v for various aging times, t_w . The red arrow points towards increasing aging times. $S_{xx}(f)$ for $t_w = 12, 22, 32, 42, 52, 62$ and 72 minutes were scaled for better visualisation. (b) The corner frequencies, f_c , calculated from Lorentzian fits to the PSDs, *vs.* t_w . (c) The zoomed-in peaks in $S_{xx}(f)$ at $f = f_{AC}$ for various aging times, t_w . The colour codes for the samples of different t_w are the same as in (a). (d) Areas under the peak in $S_{xx}(f)$ centred at $f_{AC} = 7.992$ kHz *vs.* t_w . Error bars in (b,d) are standard errors from four independent measurements.

an aqueous clay suspension of concentration 2.5% w/v, *vs.* aging time, t_w . The PSD curves at $t_w = 12, 22, 32, 42, 52, 62$ and 72 minutes were shifted vertically for better visualisation. $S_{xx}(f)$ exhibits the Lorentzian functional form as a function of frequency, besides also exhibiting a prominent peak at $f = f_{AC}$ for all t_w . We see from Fig. 6(b) that the corner frequency, $f_c = \kappa/2\pi\gamma$, of the optical trap decreases with increasing aging time, t_w , of the clay suspension. Since the change in the refractive index of the clay suspension during physical aging is expected to be negligible [43], the decreasing value of corner frequency indicates increased drag, γ , on the trapped microsphere due to the evolution of gel networks in the aging clay suspension.

We next focus on the peaks in $S_{xx}(f)$ centred at $f_{AC} = 7.992$ kHz for various clay suspension ages, t_w , in Fig. 6(c). The electric power transferred to the microsphere is equal to the area under the peak and decreases with increasing clay suspension age, t_w , at later times, as shown in Fig. 6(d). At $f > f_c$, viscous forces are expected to dominate the electric forces [29]. The decrease in electric power with increasing t_w , observed in Fig. 6(d), arises from increase in viscous damping of the trapped microsphere as the suspension viscoelasticity increases due to the gradual self-assembly of clay gel networks during the physical aging process.

We calculated the effective charge, $Q_{eff} = eZ_{eff}$, on the trapped microsphere using Eqns. (2,4) and our experimentally evaluated values of f_c and Γ for various Laponite concentrations, C_L , and aging times, t_w . The time-evolution behaviours of the effective number of elementary charges, Z_{eff} , are plotted in Fig. 7(a) as a function of t_w for different C_L . No temporal changes in Z_{eff} were seen when the microsphere was trapped in water and in a dilute clay suspension of $C_L = 0.8\%$ w/v. Interestingly,

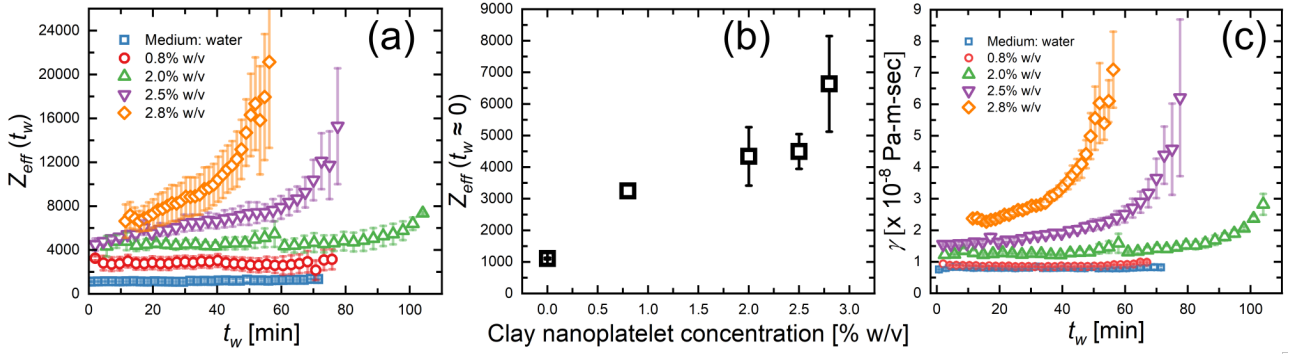


Fig. 7: (a) $Z_{eff}(t_w)$ as a function of aging time, t_w , for various Laponite clay nanoplatelet concentrations, C_L . (b) $Z_{eff}(t_w \approx 0)$ as a function of C_L and (c) the Stokes drag coefficient, $\gamma(t_w)$, characterising the trapped microsphere motion as a function of t_w for various C_L . Error bars are standard errors from three independent measurements.

when trapped in the Laponite clay sample of $C_L = 0.8\%$ w/v, the measured $Z_{eff}(t_w \approx 0)$ of the microsphere was seen to increase by a factor of three (Fig. 7(b)) when compared to its Z_{eff} measured in a water medium. We attribute the observed increase in $Z_{eff}(t_w \approx 0)$ to the transfer of net charges from the adsorbed clay nanoplatelets to the surface of the microsphere. It can be seen from Fig. 7(b) that $Z_{eff}(t_w \approx 0)$ increased further when C_L was increased. This observation can be understood by considering accelerated Laponite nanoplatelet adsorption due to their higher availability in the suspension medium. Furthermore, it is seen from Fig. 7(a) that the measured $Z_{eff}(t_w)$ increases with increasing aging time, t_w , for the higher C_L values of 2.0, 2.5 and 2.8 % w/v. We note that the increase in $Z_{eff}(t_w)$ becomes more rapid with increasing C_L . At higher C_L and t_w , higher rates of Na^+ dissolution from the faces of Laponite nanoplatelets lead to a greater reduction in the strength and range of the electrostatic repulsion between like-charged surfaces (clay nanoplatelet faces and microsphere surface) in the aqueous medium [14]. As a result of enhanced electrostatic screening at higher C_L , the formation of clay aggregates and clay gel networks get significantly accelerated. The adsorption of single clay nanoplatelets, small clay aggregates and network strands on the microsphere surface speeds up under these conditions, as manifested by the stronger temporal evolution of $Z_{eff}(t_w)$ with time.

A nanoplatelet of Laponite clay has around -700 elementary charges on its faces [44]. The charges on the rims are pH-dependent and reported to be +50 elementary charges at a pH of 9.97 at 25°C [45]. From Fig. 7(a), we record a change in $Z_{eff} \sim O(10^4)$ over the entire experimental duration. Since each Laponite nanoplatelet has $O(10^2)$ charges on its surface, our best estimate for the effective number of

adsorbed nanoplatelets is $O(10^2)$, which suggests very weak adsorption. We next calculated the Stokes drag coefficient, γ , for the trapped Latex microsphere, as a function of aging time, t_w , and plotted the data in Fig. 7(c). We see from Eqn. (4) that for $f_{AC} > f_c$, Z_{eff} and γ are both proportional to $1/f_c$. As expected under these conditions, the time-evolution of γ , as seen in Fig. 7(c), shows approximately the same temporal variation as noted earlier for Z_{eff} in Fig. 7(a).

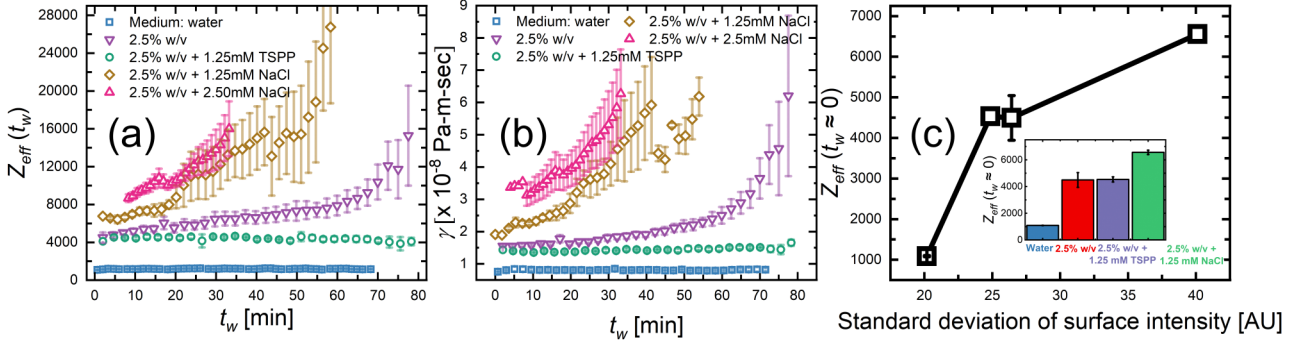


Fig. 8: (a) $Z_{eff}(t_w)$ and (b) Stokes drag coefficient $\gamma(t_w)$ as a function of aging time, t_w , for Laponite clay suspensions of concentration, $C_L = 2.5\%$ w/v prepared in pure water or in NaCl or TSPP solutions. Error bars are standard errors from three independent measurements. (c) $Z_{eff}(t_w \approx 0)$ vs. standard deviation of surface intensity in arbitrary units. (Inset) $Z_{eff}(t_w \approx 0)$ on the Latex microsphere trapped in water or clay suspensions.

Figure 8 displays the results when the microsphere was trapped in Laponite clay suspensions of concentration 2.5% w/v with and without externally added salts. Enhanced screening of the electrostatic repulsions between the microsphere and Laponite faces in the presence of NaCl results in very rapid increase in Z_{eff} (Fig. 8(a)), and therefore, also of γ (Fig. 8(b)). We attribute this observation to the accelerated adsorption of single Laponite nanoplatelets, clay aggregates and even gel network strands (Fig. 5(a)) on the microsphere [17]. The very large error bars that are seen for higher t_w , C_L and NaCl concentration imply increased heterogeneity in the adsorption process.

In the presence of TSPP, Z_{eff} does not show noticeable variation as a function of t_w . We note from Fig. 8(a) that $Z_{eff}(t_w \approx 0)$ in the presence of TSPP is higher than that for water. Since TSPP is expected to render negative charges on the rims of the nanoplatelets [22], electrostatically-driven adsorption on the weakly negatively charged microsphere can be ruled out. We conclude, therefore, that the adsorption process in this scenario is driven completely by non-electrostatic dispersion forces. In contrast, dispersion forces and electrostatic attractions are both important in the presence of NaCl. The weakened electrostatic repulsion between like-charged surfaces results in accelerated adsorption in an ionic medium, as seen from Fig. 8(a). A similar mechanism was proposed to explain the adsorption

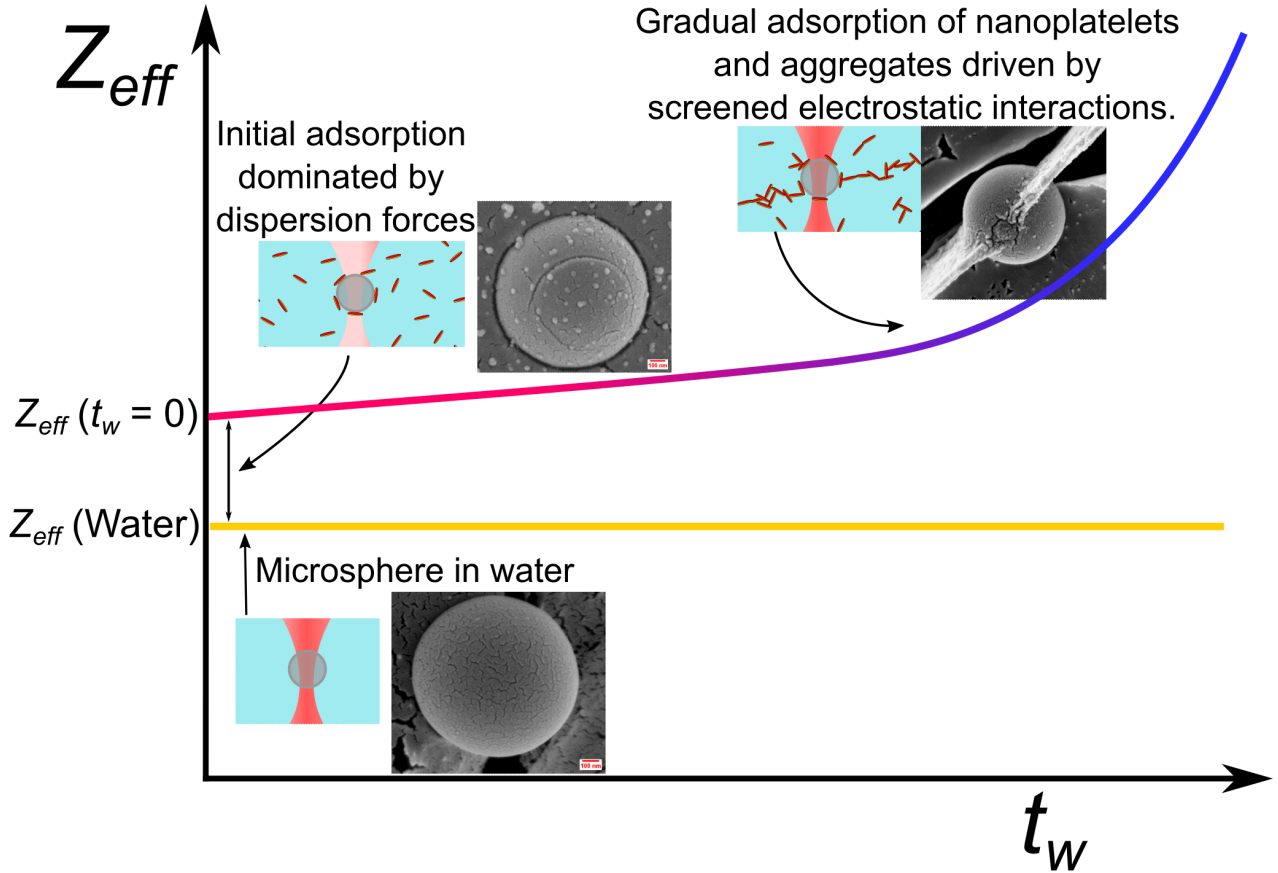


Fig. 9: Schematic representation of the mechanisms governing the adsorption process of clay nanoplatelets on a Latex microsphere.

of Laponite nanoplatelet (Grade: RDS) on polystyrene particles during emulsion polymerization [5].

We have displayed $Z_{eff}(t_w \approx 0)$ (inset of Fig. 8(c), estimated from data presented in Fig. 8(a)) as a function of the standard deviation of microsphere surface intensities (Fig. 5(b)) in Figure 8(c). The direct correlation observed between $Z_{eff}(t_w \approx 0)$ and the standard deviation of surface intensities suggests a qualitative agreement between our analyses of clay nanoplatelet adsorption on a Latex microsphere using single-colloid electrophoresis and cryo-FESEM imaging. Finally, we summarize the insights gained on the adsorption process of clay nanoplatelets on a Latex microsphere in Fig. 9. The adsorption that initially occurs is dominated by non-electrostatic dispersion interactions. When the microsphere was trapped in gel-forming clay samples above a critical concentration, the rapidly increasing $Z_{eff}(t_w)$ at later times suggests gradual adsorption of clay nanoplatelets, clay aggregates and gel network strands onto the microsphere surface, emphasising, thereby, the important role of screened electrostatic interactions.

4 Conclusions

In this report, we investigated, for the first time to the best of our knowledge, the adsorption of charged colloidal clay Laponite nanoplatelets on a preformed Latex microsphere in an aqueous medium. In a medium of $\text{pH} < 11$, a Laponite clay nanoplatelet has negatively charged faces and weakly positively charged rims [45]. Above a critical concentration of 1% w/v, these nanoplatelets self-assemble gradually to form system-spanning gel networks which reform continuously due to nanoplatelet rearrangements in a physical aging process. In the present research, we first visualised the adsorption of Laponite clay nanoplatelets on a Latex microsphere using field emission scanning electron microscopy and next quantified the kinetics of the adsorption process by performing optical tweezer-based single-colloid electrophoresis measurements.

Complex potentials can be created in optical experiments, which can be employed to study and control colloidal interactions and dynamics [46] and to verify postulates of non-equilibrium statistical mechanics [47]. In the present work, optical tweezers were used to perform sensitive measurements of the effective surface charge and Stokes drag on optically trapped Latex microspheres in aqueous suspensions of charged Laponite clay nanoplatelets in the presence of an alternating electric field. An increase in the clay nanoplatelet concentration in the suspension increased the measured effective surface charges on the trapped microsphere due to enhanced nanoplatelet adsorption. The initial adsorption process was very fast and predominantly driven by non-electrostatic dispersion forces. When the microsphere was trapped in clay suspensions of concentrations 2.0 - 2.8% w/v, we observed a non-linear increase in the effective surface charge at later times due to weakening of electrostatic repulsive interactions between the nanoplatelet faces and the surface of the trapped microsphere. Finally, we reported a very good agreement between the results obtained from cryo-FESEM and optical tweezer-based single-colloid electrophoresis.

Our work establishes optical tweezer-based single-colloid electrophoresis as a technique that has enormous potential in the study of adsorption of charged colloids on solid surfaces. This technique can be implemented successfully in applications involving colloidal stabilisation, for example, while preparing clay-armoured particles for surfactant-free Pickering emulsion polymerisation, and as a sensor for label-free detection in biomedical applications. The ability to measure small variations in the charges on a solid surface can be exploited to detect the adsorption of biomolecules. A combination of microfluidic flow cells and higher electric field strengths can be employed in future studies to attain

even better signal-to-noise ratios. This would significantly enhance temporal resolution and efficiency in the detection of macromolecular adsorption events.

Author contributions

Vaibhav Raj Singh Parmar: Methodology, Formal analysis, Investigation, Conceptualization, Writing – original draft, Software, Visualization, Writing – review & editing, Data curation. **Sayantana Chanda:** Data curation, Formal analysis, Investigation, Validation, Software, Writing – original draft, Writing – review & editing. **Sri Vishnu Bharat S:** Data curation, Validation, Investigation, Writing – original draft, Writing – review & editing. **Ranjini Bandyopadhyay:** Conceptualization, Funding acquisition, Project administration, Resources, Supervision, Visualization, Writing – review & editing.

Conflicts of interest

There are no conflicts to declare.

Data availability

The analysis codes and all the data sets related to this article are deposited in the GitHub repository (<https://github.com/vaibhav00parmar/Optical-tweezer-electrophoresis-clay-nanoplatelet-adsorption-on-Latex-microspheres-in-aqueous-media.git>).

Acknowledgements

The authors acknowledge help from Mr. K. M. Yatheendran in acquiring cryo-FESEM images and Dr. Rajkumar Biswas in fabricating the sample cells during the preliminary stage of the experiment.

References

- [1] Y. Zhang, N. W. Franklin, R. J. Chen, H. Dai, Metal coating on suspended carbon nanotubes and its implication to metal–tube interaction, *Chem. Phys. Lett.* 331 (1) (2000) 35–41. doi:[https://doi.org/10.1016/S0009-2614\(00\)01162-3](https://doi.org/10.1016/S0009-2614(00)01162-3).

- [2] G. Marzun, C. Streich, S. Jendrzey, S. Barcikowski, P. Wagener, Adsorption of colloidal platinum nanoparticles to supports: Charge transfer and effects of electrostatic and steric interactions, *Langmuir* 30 (40) (2014) 11928–11936. doi:10.1021/la502588g.
- [3] D. Matthey, J. G. Wang, S. Wendt, J. Matthiesen, R. Schaub, E. Lægsgaard, B. Hammer, F. Besenbacher, Enhanced bonding of gold nanoparticles on oxidized $\text{TiO}_2(110)$, *Science* 315 (5819) (2007) 1692–1696. doi:10.1126/science.1135752.
URL <https://www.science.org/doi/abs/10.1126/science.1135752>
- [4] A. A. Adeyemo, I. O. Adeoye, O. S. Bello, Adsorption of dyes using different types of clay: a review, *Appl. Water Sci.* 7 (2) (2017) 543–568. doi:10.1007/s13201-015-0322-y.
URL <https://doi.org/10.1007/s13201-015-0322-y>
- [5] B. Brunier, N. Sheibat-Othman, Y. Chevalier, E. Bourgeat-Lami, Partitioning of Laponite Clay Platelets in Pickering Emulsion Polymerization, *Langmuir* 32 (1) (2016) 112–124, PMID: 26653971. doi:10.1021/acs.langmuir.5b03576.
URL <https://doi.org/10.1021/acs.langmuir.5b03576>
- [6] G. Gicheva, G. Yordanov, Removal of citrate-coated silver nanoparticles from aqueous dispersions by using activated carbon, *Colloids Surf. A Physicochem. Eng. Asp.* 431 (2013) 51–59. doi:<https://doi.org/10.1016/j.colsurfa.2013.04.039>.
- [7] G. Kontogeorgis, S. Kiil, Introduction to Applied Colloid and Surface Chemistry (eds G.M. Kontogeorgis and S. Kiil), John Wiley & Sons, Ltd, 2016, Ch. 7, pp. 161–184. doi:<https://doi.org/10.1002/9781118881194.ch7>.
- [8] B. Brunier, N. Sheibat-Othman, M. Chniguir, Y. Chevalier, E. Bourgeat-Lami, Investigation of four different laponite clays as stabilizers in pickering emulsion polymerization, *Langmuir* 32 (24) (2016) 6046–6057. doi:10.1021/acs.langmuir.6b01080.
- [9] R. F. A. Teixeira, H. S. McKenzie, A. A. Boyd, S. A. F. Bon, Pickering Emulsion Polymerization Using Laponite Clay as Stabilizer To Prepare Armored “Soft” Polymer Latexes, *Macromolecules* 44 (18) (2011) 7415–7422. doi:10.1021/ma201691u.
URL <https://doi.org/10.1021/ma201691u>

- [10] T. Wang, P. J. Colver, S. A. F. Bon, J. L. Keddie, Soft polymer and nano-clay supracolloidal particles in adhesives: synergistic effects on mechanical properties, *Soft Matter* 5 (2009) 3842–3849. doi:10.1039/B904740A.
URL <http://dx.doi.org/10.1039/B904740A>
- [11] H. Van Olphen, *An Introduction to Clay Colloid Chemistry: For Clay Technologists, Geologists and Soil Scientists*. 2nd edition, Wiley, New York, 1977.
- [12] D. W. Thompson, J. T. Butterworth, The nature of laponite and its aqueous dispersions, *J. Colloid Interface Sci.* 151 (1) (1992) 236–243. doi:[https://doi.org/10.1016/0021-9797\(92\)90254-J](https://doi.org/10.1016/0021-9797(92)90254-J).
URL <https://www.sciencedirect.com/science/article/pii/002197979290254J>
- [13] K. Suman, Y. M. Joshi, Microstructure and Soft Glassy Dynamics of an Aqueous Laponite Dispersion, *Langmuir* 34 (44) (2018) 13079–13103, PMID: 30180583. doi:10.1021/acs.langmuir.8b01830.
URL <https://doi.org/10.1021/acs.langmuir.8b01830>
- [14] D. Saha, R. Bandyopadhyay, Y. M. Joshi, Dynamic Light Scattering Study and DLVO Analysis of Physicochemical Interactions in Colloidal Suspensions of Charged Disks, *Langmuir* 31 (10) (2015) 3012–3020. doi:10.1021/acs.langmuir.5b00291.
- [15] B. Ruzicka, E. Zaccarelli, L. Zulian, R. Angelini, M. Sztucki, A. Moussaïd, T. Narayanan, F. Sciortino, Observation of empty liquids and equilibrium gels in a colloidal clay, *Nature Materials* 10 (1) (2011) 56–60. doi:10.1038/nmat2921.
URL <https://doi.org/10.1038/nmat2921>
- [16] B. Ruzicka, E. Zaccarelli, A fresh look at the Laponite phase diagram, *Soft Matter* 7 (2011) 1268–1286. doi:10.1039/C0SM00590H.
URL <http://dx.doi.org/10.1039/C0SM00590H>
- [17] M. Delhorme, B. Jönsson, C. Labbez, Monte carlo simulations of a clay inspired model suspension: the role of rim charge, *Soft Matter* 8 (2012) 9691–9704. doi:10.1039/C2SM25731A.
- [18] R. Biswas, V. R. S. Parmar, A. G. Thambi, R. Bandyopadhyay, Correlating microscopic viscoelasticity and structure of an aging colloidal gel using active microrheology and cryogenic scanning electron microscopy, *Soft Matter* 19 (2023) 2407–2416. doi:10.1039/D2SM01457B.

- [19] R. Bandyopadhyay, D. Liang, H. Yardimci, D. A. Sessoms, M. A. Borthwick, S. G. J. Mochrie, J. L. Harden, R. L. Leheny, Evolution of Particle-Scale Dynamics in an Aging Clay Suspension, *Phys. Rev. Lett.* 93 (2004) 228302. doi:10.1103/PhysRevLett.93.228302.
- [20] C. Misra, V. T. Ranganathan, R. Bandyopadhyay, Influence of medium structure on the physico-chemical properties of aging colloidal dispersions investigated using the synthetic clay LAPONITE, *Soft Matter* 17 (2021) 9387–9398. doi:10.1039/D1SM00987G.
- [21] P. Mongondry, T. Nicolai, J.-F. Tassin, Influence of pyrophosphate or polyethylene oxide on the aggregation and gelation of aqueous laponite dispersions, *J. Colloid Interface Sci.* 275 (1) (2004) 191–196. doi:https://doi.org/10.1016/j.jcis.2004.01.037.
URL <https://www.sciencedirect.com/science/article/pii/S0021979704000955>
- [22] C. Martin, F. Pignon, J.-M. Piau, A. Magnin, P. Lindner, B. Cabane, Dissociation of thixotropic clay gels, *Phys. Rev. E* 66 (2002) 021401. doi:10.1103/PhysRevE.66.021401.
- [23] A. Mourchid, E. Lécolier, H. Van Damme, P. Levitz, On Viscoelastic, Birefringent, and Swelling Properties of Laponite Clay Suspensions: Revisited Phase Diagram, *Langmuir* 14 (17) (1998) 4718–4723. doi:10.1021/la980117p.
URL <https://doi.org/10.1021/la980117p>
- [24] N. Garbow, M. Evers, T. Palberg, Optical tweezing electrophoresis of isolated, highly charged colloidal spheres, *Colloids Surf. A Physicochem. Eng. Asp.* 195 (1) (2001) 227–241. doi:https://doi.org/10.1016/S0927-7757(01)00846-9.
URL <https://www.sciencedirect.com/science/article/pii/S0927775701008469>
- [25] O. Otto, C. Gutsche, F. Kremer, U. F. Keyser, Optical tweezers with 2.5kHz bandwidth video detection for single-colloid electrophoresis, *Rev. Sci. Instrum.* 79 (2) (2008) 023710. doi:10.1063/1.2884147.
- [26] G. Pesce, G. Rusciano, A. Sasso, R. Istatico, T. Sirec, E. Ricca, Surface charge and hydrodynamic coefficient measurements of bacillus subtilis spore by optical tweezers, *Colloids Surf. B* 116 (2014) 568–575. doi:https://doi.org/10.1016/j.colsurfb.2014.01.039.
URL <https://www.sciencedirect.com/science/article/pii/S092777651400040X>

- [27] G. Kokot, M. I. Bessalova, M. Krishnan, Measured electrical charge of SiO₂ in polar and nonpolar media, *J. Chem. Phys.* 145 (19) (2016) 194701. doi:10.1063/1.4967401.
- [28] G. Seth Roberts, T. A. Wood, W. J. Frith, P. Bartlett, Direct measurement of the effective charge in nonpolar suspensions by optical tracking of single particles, *J. Chem. Phys.* 126 (19) (2007) 194503. doi:10.1063/1.2734968.
- [29] F. Beunis, F. Strubbe, K. Neyts, D. Petrov, Beyond millikan: The dynamics of charging events on individual colloidal particles, *Phys. Rev. Lett.* 108 (2012) 016101. doi:10.1103/PhysRevLett.108.016101.
URL <https://link.aps.org/doi/10.1103/PhysRevLett.108.016101>
- [30] Y. Ussembayev, F. Beunis, L. Oorlynck, M. Bahrami, F. Strubbe, K. Neyts, Single elementary charge fluctuations on nanoparticles in aqueous solution, *ACS Nano* 17 (22) (2023) 22952–22959. doi:10.1021/acsnano.3c08161.
- [31] R. Grollman, G. Founds, R. Wallace, O. Ostroverkhova, Simultaneous fluorescence and surface charge measurements on organic semiconductor-coated silica microspheres in (non)polar liquids, *Opt. Express* 25 (23) (2017) 29161–29171. doi:10.1364/OE.25.029161.
URL <https://opg.optica.org/oe/abstract.cfm?URI=oe-25-23-29161>
- [32] T. Brans, F. Strubbe, C. Schreuer, K. Neyts, F. Beunis, Optical tweezing electrophoresis of single biotinylated colloidal particles for avidin concentration measurement, *J. Appl. Phys.* 117 (21) (2015) 214704. doi:10.1063/1.4922039.
- [33] T. Okada, Y. Yamamoto, T. Shibuya, H.-W. Kang, H. Miyachi, I. Karube, H. Muramatsu, J. M. Kim, Development of AC microelectrophoresis for rapid protein affinity evaluation, *Biochem. Eng. J.* 41 (1) (2008) 17–23. doi:<https://doi.org/10.1016/j.bej.2008.03.001>.
URL <https://www.sciencedirect.com/science/article/pii/S1369703X0800082X>
- [34] L. C. Geonzon, M. Kobayashi, T. Sugimoto, Y. Adachi, Adsorption kinetics of polyacrylamide-based polyelectrolyte onto a single silica particle studied using microfluidics and optical tweezers, *J. Colloid Interface Sci.* 630 (2023) 846–854. doi:<https://doi.org/10.1016/j.jcis.2022.10.067>.
URL <https://www.sciencedirect.com/science/article/pii/S0021979722018288>

- [35] J. A. van Heiningen, R. J. Hill, Polymer adsorption onto a micro-sphere from optical tweezers electrophoresis, *Lab Chip* 11 (2011) 152–162. doi:10.1039/C005217P.
- [36] E. Bianchi, R. Blaak, C. N. Likos, Patchy colloids: state of the art and perspectives, *Phys. Chem. Chem. Phys.* 13 (2011) 6397–6410. doi:10.1039/C0CP02296A.
- [37] S. F. Tolić-Nørrelykke, E. Schäffer, J. Howard, F. S. Pavone, F. Jülicher, H. Flyvbjerg, Calibration of optical tweezers with positional detection in the back focal plane, *Rev. Sci. Instrum.* 77 (10) (2006) 103101. doi:10.1063/1.2356852.
- [38] K. C. Neuman, S. M. Block, Optical trapping, *Rev. Sci. Instrum.* 75 (9) (2004) 2787–2809. doi:10.1063/1.1785844.
- [39] T. A. Wood, G. S. Roberts, S. Eaimkhong, P. Bartlett, Characterization of microparticles with driven optical tweezers, *Faraday Discuss.* 137 (2008) 319–333. doi:10.1039/B703994H.
- [40] I. Semenov, O. Otto, G. Stober, P. Papadopoulos, U. Keyser, F. Kremer, Single colloid electrophoresis, *J. Colloid Interface Sci.* 337 (1) (2009) 260–264. doi:https://doi.org/10.1016/j.jcis.2009.05.017.
URL <https://www.sciencedirect.com/science/article/pii/S0021979709006602>
- [41] G. Pesce, V. Lisbino, G. Rusciano, A. Sasso, Optical manipulation of charged microparticles in polar fluids, *Electrophoresis* 34 (22-23) (2013) 3141–3149. doi:https://doi.org/10.1002/elps.201300214.
- [42] V. R. Singh Parmar, R. Bandyopadhyay, Manipulating crack formation in air-dried clay suspensions with tunable elasticity, *arXiv e-prints* (2024) arXiv:2407.01396arXiv:2407.01396, doi:10.48550/arXiv.2407.01396.
- [43] N. Ravi Kumar, K. Muralidhar, Y. M. Joshi, On the refractive index of ageing dispersions of Laponite, *Appl. Clay. Sci.* 42 (1) (2008) 326–330. doi:https://doi.org/10.1016/j.clay.2007.12.010.
- [44] S. Kutter, J.-P. Hansen, M. Sprik, E. Boek, Structure and phase behavior of a model clay dispersion: A molecular-dynamics investigation, *J. Chem. Phys.* 112 (1) (2000) 311–322. doi:10.1063/1.480582.
URL <https://doi.org/10.1063/1.480582>

- [45] S. L. Tawari, D. L. Koch, C. Cohen, Electrical double-layer effects on the brownian diffusivity and aggregation rate of laponite clay particles, *J. Colloid Interface Sci.* 240 (1) (2001) 54–66. doi:<https://doi.org/10.1006/jcis.2001.7646>.
- [46] D. Saha, S. Tarama, H. Löwen, S. U. Egelhaaf, Cybloids – creation and control of cybernetic colloids, *Soft Matter* 20 (2024) 8112–8124. doi:[10.1039/D4SM00853G](https://doi.org/10.1039/D4SM00853G).
URL <http://dx.doi.org/10.1039/D4SM00853G>
- [47] S. Ciliberto, Experiments in stochastic thermodynamics: Short history and perspectives, *Phys. Rev. X* 7 (2017) 021051. doi:[10.1103/PhysRevX.7.021051](https://doi.org/10.1103/PhysRevX.7.021051).
URL <https://link.aps.org/doi/10.1103/PhysRevX.7.021051>

Supplementary Material

Using optical tweezer electrophoresis to investigate clay nanoplatelet adsorption on Latex microspheres in aqueous media

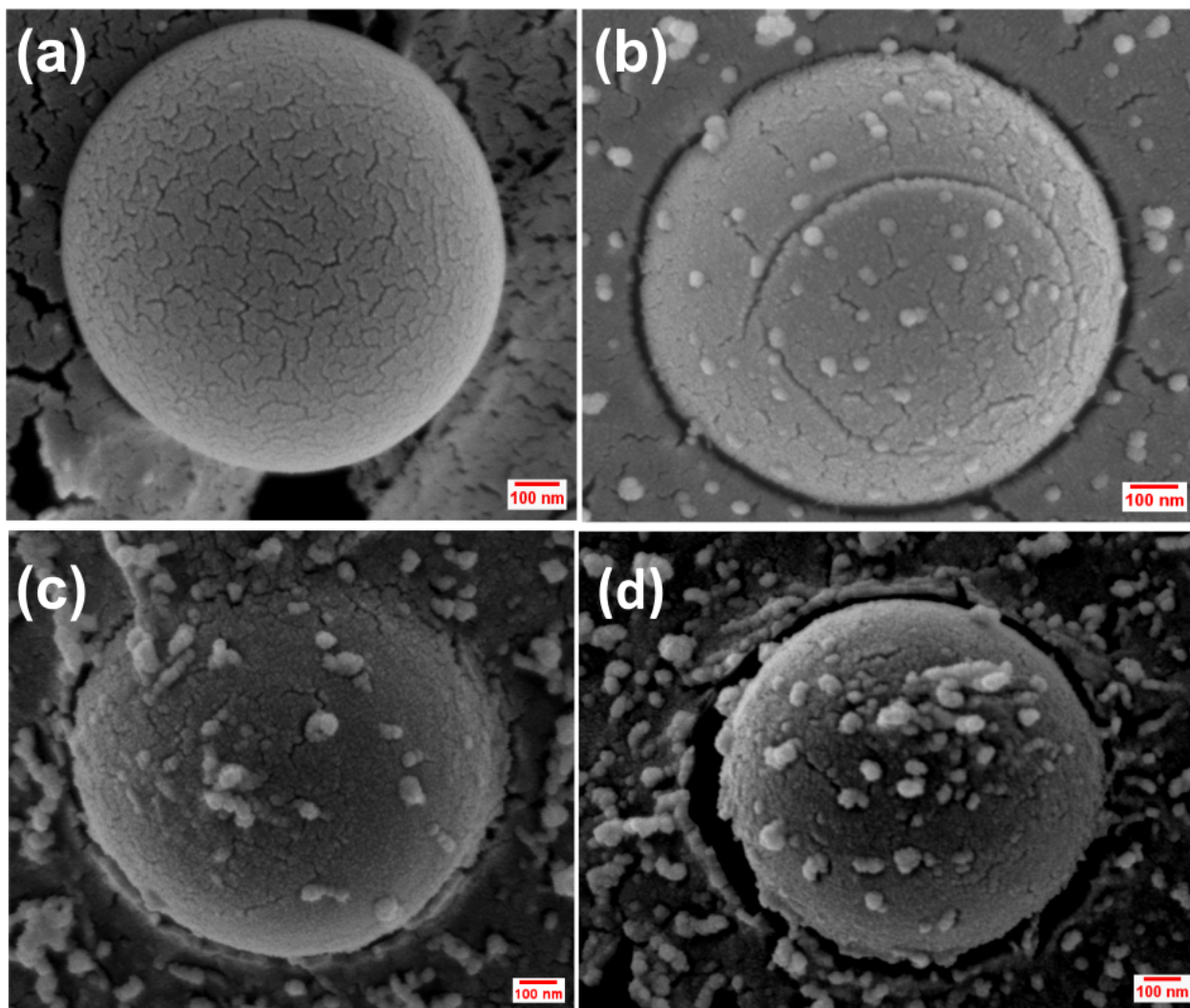
Vaibhav Raj Singh Parmar, Sayantan Chanda, Sri Vishnu Bharat Sivasubramaniam and Ranjini Bandyopadhyay*

Soft Condensed Matter Group, Raman Research Institute, C. V. Raman Avenue, Sadashivanagar, Bangalore 560 080, INDIA

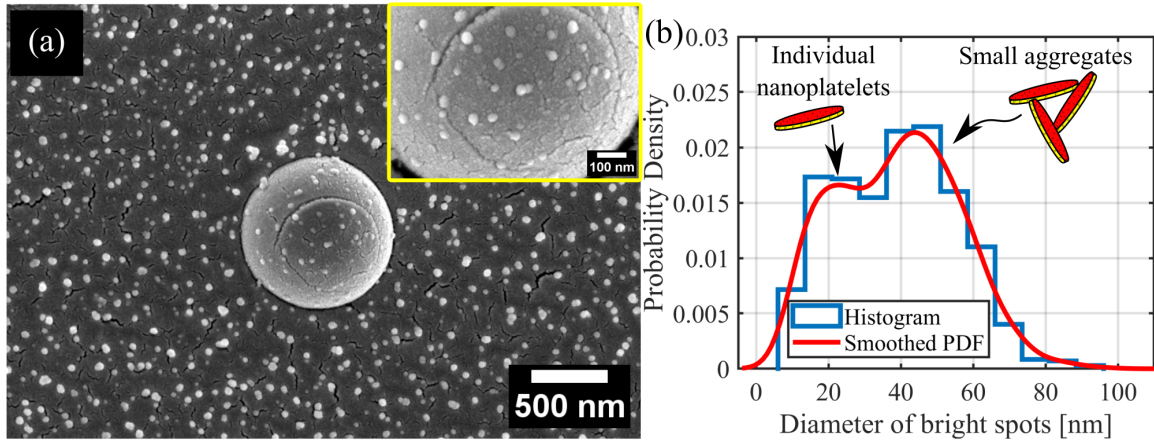
November 11, 2024

*Corresponding Author: Ranjini Bandyopadhyay; Email: ranjini@rri.res.in

ST1 Cryogenic field emission scanning electron microscopy (cryo-FESEM) images of Latex microsphere



Supplementary Fig. S1: Raw cryo-FESEM images of a trapped Latex microsphere in (a) pure water, (b) an aqueous Laponite suspension of concentration 2.5% w/v, (c) an aqueous Laponite suspension with 1.25 mM NaCl and (d) an aqueous Laponite suspension with 1.25 mM TSPP.



Supplementary Fig. S2: (a) Cryo-FESEM image of a Latex microsphere (diameter = 1 μm) suspended in a clay suspension of concentration 2.5% w/v at aging time $t_w = 90$ minutes. (Inset) Higher magnification image of the Latex microsphere surface. Many bright spots can be seen on the surface of the microsphere. (b) Histogram and smoothed probability density of the diameters of 932 bright spots identified from (a) using ImageJ and estimated using the histogram and ksdensity functions in MATLAB@2024. The diameter of each bright spot was estimated from its area, A_{spot} , by calculating $2\sqrt{A_{spot}/\pi}$. The peak in the probability density function at ~ 25 nm corresponds to an individual clay nanoplatelet, while the second peak at a larger diameter corresponds to small clay aggregates

ST2 Calibrations of the optical tweezer

ST2.1 Measurement of QPD sensitivity

The QPD sensitivity, β , determined from the uncalibrated power spectrum, S_{vv} , of the trapped microsphere in QPD units, is related to the position of the microsphere as follows: $x = \beta x_v$, where x_v is the position of the microsphere in QPD units. The power spectrum of the particle is given by:

$$S_{xx} = \int_{-\infty}^{\infty} e^{-i\omega t} \int_{-\infty}^{\infty} x(t)x(t+\tau) d\tau dt \quad (\text{S1})$$

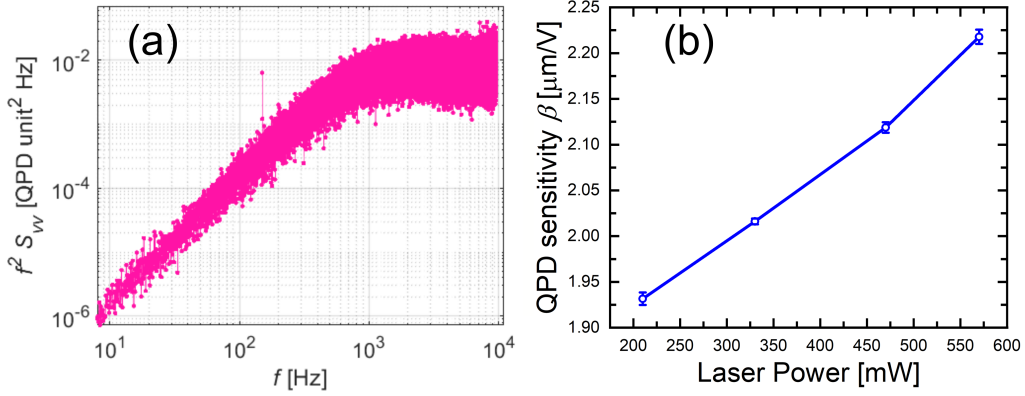
Therefore, $S_{xx} = \beta^2 S_{vv}$. For a trapped Brownian particle, S_{xx} is theoretically calculated from the first term in Eqn. (2) of the main manuscript:

$$S_{xx} = \beta^2 S_{vv} = \frac{k_B T}{\pi^2 \gamma (f_c^2 + f^2)} \quad (\text{S2})$$

For frequencies $f \gg f_c$,

$$f^2 S_{vv} = \beta^{-2} \frac{k_B T}{\pi^2 \gamma} \quad (\text{S3})$$

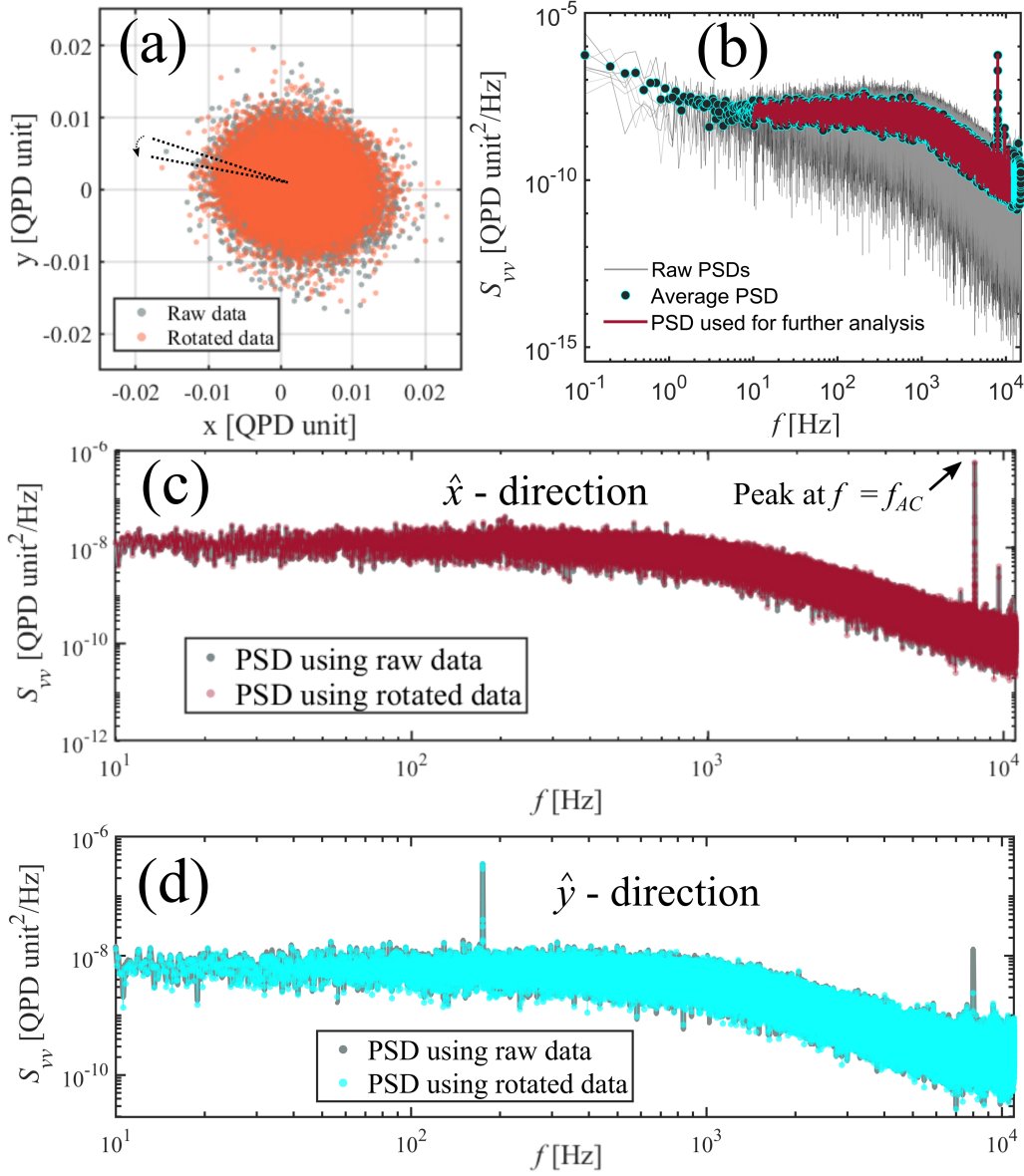
This indicates that $f^2 S_{vv}$ attains a constant value at high frequencies. For a microsphere trapped in water, the plateau is clearly visible in Fig. S3(a). Since the Stokes drag coefficient $\gamma = 6\pi\eta a$, where a is the radius of the microsphere, η is the medium viscosity and T is temperature of the medium, is known for a microsphere in water, QPD sensitivity, β , can be determined using Eqn. (S3). This method is less prone to errors as the possibility of experimental noise at lower frequencies is eliminated. QPD sensitivity, β , evaluated at various laser powers is plotted in Fig. S3(b).



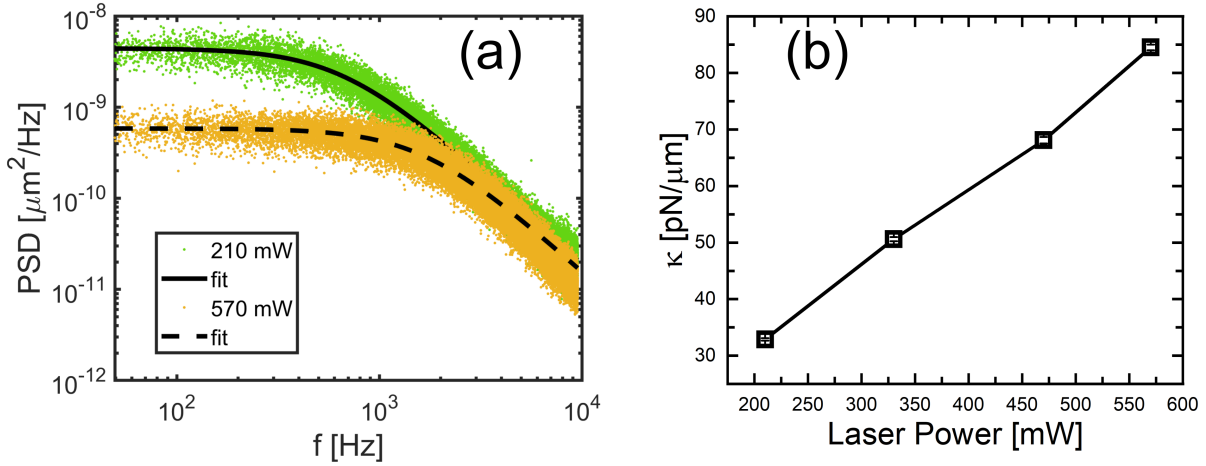
Supplementary Fig. S3: (a) $f^2 S_w$ as a function of f for a microsphere trapped in water. (b) QPD sensitivity, β vs. laser power. The error bars represent the standard errors estimated from 11 microspheres trapped in water.

ST2.2 Calculation of power spectral density (PSD) from the position fluctuations of a trapped Brownian microsphere

Figure S4(a) shows the thermal fluctuations of a trapped microsphere. We acquired the time-dependent position fluctuations of an optically trapped microsphere for a period of 70 minutes. We divided this data into equally-spaced datasets containing position fluctuations acquired for 80 seconds. The dataset containing position fluctuations for 80 seconds was further divided into 10 sub-datasets with equally-spaced data. The power spectral density (PSD) for each sub-dataset was estimated using the periodogram function in MATLAB as shown by grey curves in Fig. S4(b). 10 power spectral density curves were extracted to compute an average (black circles in Fig. S4(b)). Since there can be noise and aliasing effects at low and high frequencies, power spectral densities in a frequency range of 10 to 11000 Hz were used for further analysis (Figs. S4(c,d)). The peak observed near 200 Hz in Figs. S4(c,d) was identified as environmental noise from the laboratory and eliminated. Despite carefully positioning the sample cell on the sample holder, a slight misalignment still existed between the direction of the applied field and the horizontal axis of the QPD. The slight misalignment resulted in a weak peak at $f = f_{AC}$ in the PSD along the \hat{y} -direction. We resolved this issue during data analysis by rotating the position fluctuation data until the electric field direction was perfectly aligned with the horizontal axis of the QPD. This reduces complexity in further analysis.



Supplementary Fig. S4: (a) Scatter plot showing position fluctuations of the trapped microsphere. The data is rotated by an angle < 0.15 rad to align the electric field with the horizontal axis of the QPD. (b) Power spectral densities of individual sub-datasets, average power spectral density, and cropped power spectral density used for further analysis. (c,d) Power spectral densities along \hat{x} and \hat{y} directions respectively, computed from raw and rotated position fluctuations. It is seen from (d) that rotation eliminates the $f = f_{AC}$ peak from the \hat{y} -direction.



Supplementary Fig. S5: (a) PSDs for a trapped microsphere in water at two different laser powers and the Lorentzian fits to the data (black lines). (b) Changes in trap stiffness with laser power.

ST2.3 Calibration of trap stiffness

The stiffness of the optical trap was calculated using the power spectral density method. A Latex microsphere of size $1\mu\text{m}$ was trapped in water using an optical tweezer at a desired laser power. The microsphere was trapped at approximately $8\mu\text{m}$ above the bottom surface to eliminate wall effects. The calculated power spectral density, $S_{xx}(f)$, of the centre of mass fluctuations of the trapped particle was fitted to a Lorentzian function:

$$S_{xx} = \frac{k_B T}{\pi^2 \gamma (f_c^2 + f^2)}$$

Data and fits for two different laser powers are shown in Fig. S5(a). The corner frequencies $f_c = k/2\pi\gamma$ were extracted from the fits. Using the fitted value of f_c and the estimated value of the Stokes drag coefficient $\gamma = 6\pi\eta a$, the trap stiffness κ was determined for four different laser powers. The trap stiffness shows a linear increase with laser power, as shown in Fig. S5(b).